RSC Advances

ROYAL SOCIETY OF CHEMISTRY

www.rsc.org/advances

the Pt NPs into Pt dendrites on indium tin oxide (ITO) thin film based on diffusion-limited aggregation (DLA) theory; 2) the appearance of nanospheres through a coordination interaction between the amine ligand of metalloporphyrin and Pt nanostructures. Nevertheless, for another kind of Pt NPs surrounded by citrate ions, we didn't achieve the dendritic structures and nanospheres under the same condition, due to the effect of citrate ions obstruction, demonstrating the easily approachable surfaces of Pt nanostructures were obtained in our system. The Pt nanostructures with active and "clean" surface are recommended to be applied in the fields of nanoelectronics, sensors and catalysis, which may strongly improve their performances. Furthermore, the Pt dendritic structures and metalloporphyrin/Pt nanospheres might have potential for the development of advanced functional materials, and the two kinds of assembly processes can be manipulated for different purposes.

2. Materials and methods

2.1 Materials

$H_2PtCl_6 \cdot 6H_2O$, methanol, Sn (IV) meso-tetra (4-pyridyl) porphine dichloride and ITO electrodes were purchased from Sigma-Aldrich Company and used as received. Distilled water was used throughout and other chemicals were of reagent grade.

2.2 Apparatus

Scanning electron microscopy (SEM) of the nanostructures was carried out on a Zeiss Gemini 1550 device. High resolution transmission electron microscopy (TEM) was performed using an FEI TITAN 80-300 microscope with a Cs-image corrector operated at 300kV. The electrochemical experiments were conducted with a three-electrode setup controlled by a potentiostat (AUTOLAB, The Netherlands). The three-electrode systems were composed of a Pt NPs modified ITO thin-film working electrode, a platinum coil counter electrode and an Ag/AgCl reference electrode (3 M KCl, Ef = 0.210 V vs NHE). The measurement of the zeta potential was performed in an aqueous medium by using a dynamic light scattering system Zetasizer Nano ZS (Malvern Instruments). UV-visible absorption spectra were obtained with a Perkin-Elmer Lambda 900 instrument. X-ray photoelectron spectroscopy (XPS) data was carried out using a PHI 5000 VersaProbe II (ULVAC-PHI Inc., USA) equipped with a monochromatic Al Kalpha X-ray source operating at 100 W and 20 kV, with the compounds determined with the help of a NIST database. A 150 W Xenon Arc lamp (Oriel Instruments, Model No. 6255) was applied for illumination during the photoreduction process.

2.3 Synthesis of Pt NPs with photoreduction method

12 mg of $H_2PtCl_6 \cdot 6H_2O$ was mixed with 2 mL of methanol in 38 mL distilled water added to the vessel. The mixture was then purged with nitrogen gas for half an hour to drive away the residual air and exposed to the light of the 150 W Xenon Arc lamp (Oriel Instruments, Model No. 6255) without a light filter for 4 hours with stirring until the color of the solution changed from a yellowish to a brown color. The reaction was carried out under a fuming hood with a PMMA window.

2.4 Formation of the dendritic Pt nanostructures with appropriate addition and evaporation of water

10 µL of the as-prepared Pt NPs solution was dropped on the surface of ITO thin film, after drying, with 10 µL distilled water dropped on the same place with the Pt NPs. This process was repeated 3 times. Finally, the SEM images were obtained from the self-assembled dendritic Pt nanostructures on the ITO thin film.

2.5 Formation of the nanospheres between the Pt nanoparticles and metalloporphyrin

5 mL of 300 µM aqueous solutions of Sn (IV) meso-tetra (4-pyridyl) porphine dichloride, 10 mL Pt NPs solution and 10 mL distilled water were rapidly mixed and then left undisturbed at room temperature for different times.

3. Results and discussion

3.1 Characterization of Pt nanostructures

3.1.1 Morphological characterization of Pt nanostructures

During the photochemical synthesis process, the Pt (IV) ions were reduced to Pt (II) and Pt (0) by free radicals produced from the electron donor methanol under UV irradiation and then Pt (0) condensed to form nuclei. Once stable nuclei were formed, they could increase in size and produce further Pt NPs.

The morphology of the as prepared Pt NPs is illustrated in figure 1 by SEM and TEM images. An overview SEM image of the product in figure 1a exhibits the Pt NPs with an average size of approximately 15 nm, while the corresponding high resolution TEM image in figure 1b reveals that the polycrystalline Pt NPs were formed by densely packed grains. An enlarged high resolution TEM image of an individual Pt NP (inset of figure 1b) displays lattice fringes with an interplanar distance of about 0.227 nm, corresponding to the interplanar spacing of Pt (111) planes.

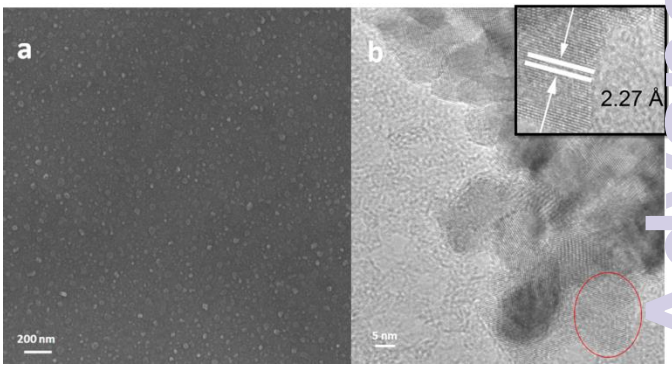

Figure 1. (a) SEM and (b) TEM images of the as prepared Pt NPs. Inset of (b): high-resolution TEM image of individual Pt NP showing lattice fringes.

The formation procedure of the Pt NPs is shown by the SEM images of the intermediate products at 5 minutes (a), 20

minutes (b) and 4 hours (c), respectively (figure S1). At the beginning, few small Pt NPs with an average diameter of about 10 nm formed, as is displayed in figure S1 (a); more and more Pt NPs were then produced with the increasing reaction time illustrated in figure S1 (b). Due to their higher energy, induced by a larger surface-to-volume ratio and higher collision frequency associated with their greater mobility, the coalescence or attachment of small Pt NPs produced larger Pt NPs, as can be observed in figure S1 (c), thus the decrease in surface energy was obtained by eliminating pairs of surfaces that supplied a strong thermodynamic driving force for particle coalescence.[24-26]

3.1.2 Zeta-potential measurement of Pt nanostructures

Measurement of the zeta-potential showed that the as prepared Pt NPs were negatively charged in the medium with a zeta-potential (ζ) of −32 mV, indicating that the chloride ions surrounding the Pt NPs can prevent these from aggregating in a short period of time.

3.1.3 UV-visible absorption spectra studies of Pt nanostructures

UV-visible absorption spectra of the intermediate products obtained at 0 minute (a), 10 minutes (b) and 4 hours (c) of the irradiation process are exhibited in figure 2. As is apparent in the insert, two broad-range peaks of the platinum complex appear at 375 nm and 465 nm at zero reaction time.[27] After 10 minutes' exposure to light, these peaks decreased significantly, as is shown in figure 2 (b), indicating that the Pt photoreduction took place in the first 10 minutes. Finally, these two peaks completely disappeared after 4 hours' irradiation, shown in figure 2 (c), indicating that the Pt photoreduction process was completed.

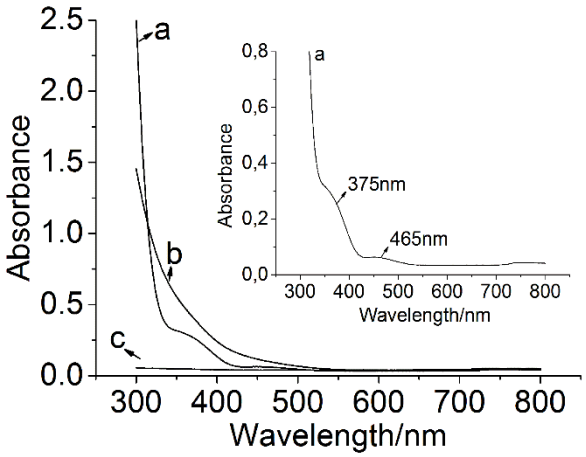

Figure 2. UV-visible absorption spectra of the intermediate product solutions obtained at 0 min (a), 10 min (b) and 4 hours (c) during the formation procedure of the Pt nanostructures.

3.1.4 Catalytic activity characterization of Pt nanostructures

The catalytic activity of the Pt NPs drop casted on the ITO thin film substrate for hydrogen evolution reactions was characterized in a 0.1 M $HClO_4$ solution with a typical three-electrode cell set-up. As is shown in figure S2 (a), the cyclic voltammetric curves reveal strong hydrogen adsorption and desorption peaks in the potential range of 0 - 0.4 V recorded against NHE on the surface of the Pt NPs, and the electrochemically active area of Pt can be calculated by integrating the cathodic current for the hydrogen adsorption reaction, correcting for the "double-layer" charging current.[28] Additionally, we used the clean polycrystalline Pt electrode charge density of 210 μC cm^{-2} in the calculation, which has been reported in the previous work by supposing the adsorption of one H atom per Pt atom.[29] The finally calculated active area of the Pt NPs was 8.09 cm^2 (The concentration of Pt NPs measured by inductively coupled plasma mass spectrometry was 0.00121 mg/cm^2). And the active surface area normalized current density, j, as a function of the potential was presented in figure S2 (b). As can be seen in figure S2 (b), Pt NPs can drive a large catalytic current density at low potential, indicating the high degree of activity of the Pt NPs in the hydrogen evolution reaction. As is known, an electro-catalyst with high intrinsic activity towards a specific redox process is characterized by a low Tafel slope.[30] Thus, the corresponding Tafel plot of the Pt NPs was investigated and is displayed as the inset of figure S2 (b). According to previous publications, the Pt catalysts of the hydrogen evolution reaction usually demonstrate small Tafel slopes.[31-36] In our results, the Pt NPs display a Tafel slope of 66.5 mV/dec, showing relatively fast kinetics in driving the hydrogen evolution reaction, leading to the high catalytic performance.

3.2 Self-assembly of Pt NPs into Pt dendritic structures

In order to assess the surface activity, the as synthesized Pt NPs were dropped on the surface of an ITO thin film and treated by an appropriate addition and evaporation of water. Perfect dendritic structures were formed on the ITO film and the morphology of the self-assembled dendritic Pt nanostructures was characterized by SEM, shown in figure 3. The presence of abundant pine-like shapes with multiple branches is illustrated in figure 3 (a) and each branch is mostly composed of clusters of aggregated Pt NPs in figure 3 (b). We assumed that the evaporation of water may force the Pt NPs to move together and aggregate, leading to the formation of an original self-assembly. With the further evaporation, some single Pt NPs move at random and coalesce when they meet the primeval self-assembly in a limited region. The mechanism of self-assembled dendritic Pt nanostructure formation can be explained by diffusion-limited aggregation (DLA) theory.

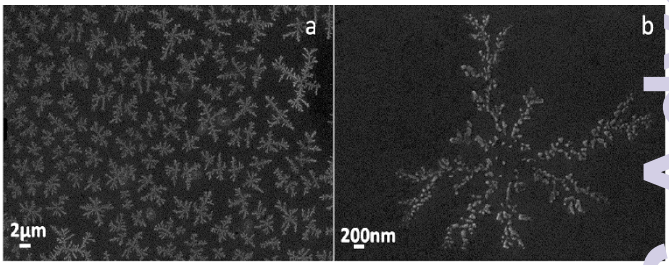

Figure 3. SEM images of the self-assembled dendritic Pt nanostructures (a), enlarged view of one dendritic Pt nanostructure (b).

Witten and Sander presented one of the first computational works supporting dendritic growth with DLA theory in 1981.[37] DLA theory was proposed as an idealization of the process whereby particles are subject to random walks due to Brownian motion and cluster together to form dendrite aggregates, whereby the rate-limiting step is a diffusion of particles to aggregates.[37] Thus, we propose a self-assembly mechanism by which the as prepared Pt nanostructures are transformed into nanodendrites based on DLA theory. Firstly, a Pt seed is located in the original area, while the second Pt particle is near this area. Then, the second Pt particle walks randomly with the evaporation of water until it meets a site adjacent to the seed, becoming a part of the primitive self-assembly. Lastly, the structure grows as more Pt NPs adhere, with the exposed ends of the structure tending to increase more rapidly than at other perimeter sites because those near the center are "shadowed" and the new particles prefer the regions that protrude away from the main structure, giving rise to the dendritic structures.[38] The number of Pt NPs decreased with prolonged reaction times and they finally disappeared entirely, leaving behind Pt nanodendrites, thereby showing that growth proceeded through particle attachment.[39] This observed "enhanced" diffusion to the tips is similar to the spherical diffusion of metal-cations at the end of tips during the electrochemical growth of the metallic dendrites.[40] Recently, the Alivisatos group applied a simple random walk model to describe the dendritic assembly of alkanethiol-capped gold NPs on a glassy carbon support during the electrochemical reduction of protons and CO_2, and the period of a fractal aggregation was confirmed by random branching.[41]

The dendritic Pt nanostructure has spurred much research in a wide variety of technological fields, because the dendritic structures have the rich edges and corner atoms derived from the high structural complexity, which are favourable for decreasing the Pt consumption, supplying high surface area and enough absorption sites for involved molecules in a narrow space, and promoting improved performance in catalytic applications. For example, the dendritic Pt provided higher performance, larger electrochemical surface area and improved diffusion characteristics compared to a conventional sputtered Pt film when it was assembled on the electrode surface as the cathode catalyst layer for a single fuel cell, and the activity on unit electrochemical surface area of the dendritic Pt was higher than that of Pt/C.[42] The spontaneously assembled three-dimensional dendritic Pt NPs prepared by a non-templated sonoelectrochemical method, exhibited improved electrochemical catalytic behavior for the oxidation of methanol and glucose with respect to the monodisperse Pt nanoparticles, due to the porosity structure and the greatly enhanced effective surface area.[20] In Shelnutt's work, 2-D and 3-D dendritic Pt nanostructures were synthesized by means of a seeding/autocatalytic approach, which showed photocatalytic activity for H_2 evolution from water.[43] The surfactant-free dendritic Pt NPs catalysts exerted particular catalytic activity in both methanol oxidation and p-nitrophenol reduction.[44] Therefore, we expect that the self-assembled dendritic Pt nanostructures in our work would be useful for sensing and catalytic application.

In contrast to the Pt NPs prepared using the photoreduction method, another type of Pt NP was synthesized with the citrate reduction method,[45] having been treated with the addition and evaporation of water under the same condition. (The details of the synthetic procedure are provided in the supporting information). The formation mechanism of the Pt NPs with the citrate reduction method is based on the reduction of Pt ions through sodium citrate to form the small Pt NPs that are surrounded by citrate ions. Figure S3 shows the SEM images of the Pt NPs synthesized using the citrate reduction method (a) without and (b) after the addition and evaporation of water. In figure S3 (a), the Pt NPs through the citrate reduction method are almost monodisperse, with a mean particle size of 5 nm, whereas the Pt dendrites are not shown in figure S3 (b) after the addition and evaporation of water, implying that the citrate ions blocked the Pt NP interface for this kind of self-assembly more efficiently than chloride ions, which may be adsorbed by Pt NPs prepared using the photoreduction method. On the other hand, this result proved that the Pt NPs synthesized by the photoreduction method have "clean" and active surfaces, allowing them to form the dendrite structure through interaction between each other based on the DLA theory.

3.3 Coordination-driven assembly between metalloporphyrin and Pt NPs

The thermodynamically unstable and readily accessible surface of the Pt NPs prepared with the photoreduction method was further evinced by interaction with Sn (IV) meso-tetra (4-pyridyl) porphine dichloride (figure 4). When mixed, the Pt NPs and the aqueous solutions of Sn (IV) meso-tetra (4-pyridyl) porphine dichloride produced the nanospheres due to the coordination reaction between the nitrogen ligand of metalloporphyrin and Pt NPs. The formation procedure of these nanospheres is revealed by SEM images of the intermediate products at 3 hours (a), 4.5 hours (b), 7 hours (c) and 24 hours (d), respectively (figure 5). As is illustrated in figure 5 (a), few nanospheres formed on the surface of the Pt nanostructures after 3 hours of reaction and both the amount and diameter of nanospheres increased after 4.5 hours and 7 hours' reaction, as displayed in figure 5 (b) and (c), respectively. In addition, a lot of solid nanospheres, with an average diameter of about 250 nm, are exhibited in figure 5 (d) and the surfaces of the nanospheres are decorated with aggregated Pt nanostructures, indicating the number and size of nanospheres that could be controlled by modification of the reaction time.

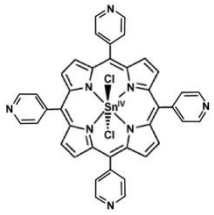

Figure 4. The structure of Sn (IV) meso-tetra (4-pyridyl) porphine dichloride.

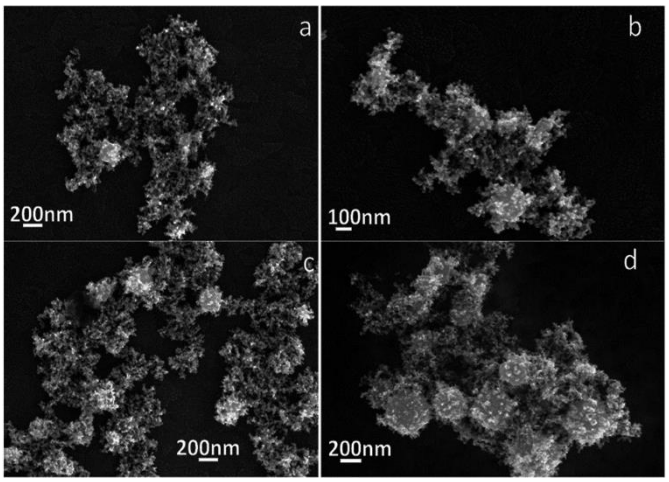

Figure 5. SEM images of the intermediate product solutions obtained at 3 hours (a), 4.5 hours (b), 7 hours (c) and 24 hours (d) during the reaction between Sn (IV) meso-tetra (4-pyridyl) porphine dichloride and Pt nanostructures prepared by means of the photoreduction method.

In a study in 2001, Watabe et al.[46] described how nitrogen ligand can coordinate with Pt (IV) cation by forming Pt (IV) complexes with dipeptide. After four years, a novel coordination-induced formation at the submicrometer-scale, monodisperse, spherical colloids of organic-inorganic hybrid materials was presented as a coordination-based assembly between the nitrogen ligand of p-phenylenediamine and Pt cations in an aqueous solution at room temperature.[47] Another monodisperse nanosphere was reported in 2008 through the coordination of polymerization tetrakis (4-pyridyl) porphyrin–metal complexes with H_2PtCl_6 in an aqueous solution; these nanocomposites have potential applications in catalysis and solar energy conversion systems.[48] Nevertheless, all of the afore-mentioned coordinate reactions between Pt and nitrogen-containing molecules were concentrated on Pt ions, rather than Pt (0)-NPs. According to these previous publications, two possible explanations were conjectured to explain the production of the nanosphere/Pt metal nanocomposites in our system: 1) some non-reduced Pt (IV) or Pt (II) cations were probably adsorbed on the surface of Pt (0)-NPs and initiated the formation of these solid nanospheres through coordination with pyridyl-groups of porphyrins; 2) Pt (0)-NPs could participate in the formation of nanospheres due to the coordination interaction of Pt (0)-NPs with nitrogen-containing molecules like pyridine.

Whether there exist Pt ions in the Pt NPs solution following photoreduction synthesis and purification was investigated by means of XPS. The results of XPS applied to the mixture of H_2PtCl_6 and methanol both before (a) and after (b) photoreduction synthesis and the nanospheres formed by the coordination reaction between nitrogen ligand of metalloporphyrin and Pt NPs (c) are displayed in figure 6. Firstly, the precursor of the Pt nanostructure contains mainly Pt (IV) (Pt (IV) 4f 7/2 = 74.4 eV, 4f 5/2 = 77.9 eV) with a small part of Pt (II) (Pt (II) 4f 7/2 = 72.6 eV, 4f 5/2 = 76.1 eV) and the ratio of the areas of Pt (IV): Pt (II) is 2:1 (see figure 6 (a)). The appearance of Pt (II) may be attributed to the reduction reaction of Pt (IV) through X-ray irradiation during the collection of the XPS spectrum.[47] Following the photoreduction process, the XPS spectrum of the Pt nanostructure indicates two energy peaks in the Pt 4f region, at 70.8 and 74.3 eV in figure 6 (b), implying that all the Pt ions were reduced to Pt (0)-NPs. Finally, XPS data for the nanospheres of metalloporphyrin and Pt confirms that these consist primarily of Pt (0), and that the energies were Pt (0) 4f 7/2 = 70.9 eV and 4f 5/2 = 74.3 eV in figure 6 (c). Thus, the second speculation, that Pt (0)-NPs are involved in the formation of nanospheres owing to interaction between Pt (0)-NPs and pyridyl-groups of porphyrins, is more reasonable for explaining the production of these nanosphere/Pt metal nanocomposites, meaning that all of the Pt ions were reduced to Pt (0)-NPs during the photoreduction process.

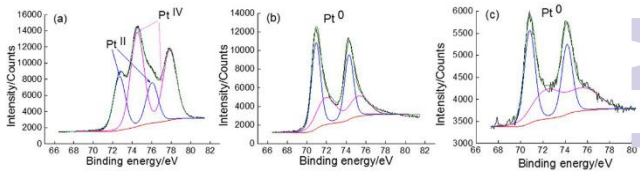

Figure 6. The XPS spectrum of the mixture of H_2PtCl_6 and methanol before (a) and after (b) photoreduction synthesis and the nanospheres formed by means of the coordination reaction between the nitrogen ligand of metalloporphyrin and Pt NPs (c).

By contrast, the nanosphere/Pt metal nanocomposites were not found in the mixture of Pt NPs prepared with the citrate reduction method[45] and metalloporphyrin molecules under the same condition, indicating that the citrate ions surrounded and stabilized the Pt NPs again, inhibiting the coordination reaction between Pt NPs and pyridyl-groups of porphyrins. In this respect, the easily accessible and active surface of the Pt NPs synthesized through the photoreduction method has been further verified, providing additional opportunities for the coordination interaction between Pt NPs and amine-containing molecules, as well as various post-synthetic building block assemblies.

4. Conclusions

In summary, we applied a simple but efficient strategy for the preparation of Pt NPs with a “clean” and active surface via the photoreduction process in an aqueous solution without using any organic solvents and surfactants as structure-protecting and directing agents. The catalytic activity of the Pt NPs was characterized by polarization curves and Tafel plots, showing that relatively fast kinetics drive the hydrogen evolution reaction. The easily accessible surface of the as synthesized Pt nanostructures was demonstrated by the following effects: 1) the self-assembly of the Pt NPs into Pt dendrites on ITO thin film based on DLA theory; 2) the appearance of nanospheres through a coordination interaction between the amine ligand of metalloporphyrin and Pt nanostructures. However, these two phenomena were not found in another kind of Pt NPs surrounded by citrate ions, because the citrate ions inhibited the Pt NPs from coming into contact with other molecules. Th

results provide evidence that citrate ions have a stronger stabilization effect on Pt NPs than chloride ions and confirm the active and easily approachable surface of Pt nanostructures prepared by means of the photoreduction process. In future, this kind of Pt nanostructures may have potential application in the fields of nanoelectronics, sensors and catalysis, given its "clean" surface and high surface area, which may greatly improve its performance, while the described formation routes of Pt dendrites and metalloporphyrin/Pt nanospheres might have potential for the development of advanced functional materials. Furthermore, much attention should be paid to the prevention of catalyst poisoning if the Pt structures have similar clean and easily accessible surfaces.

Acknowledgements

We kindly thank Dr. M Heggen and M Gocyla for the TEM investigation, Dr. A Besmehn for the XPS study, and Dr. A Csiszar for zeta-potential and hydrodynamic radius distribution investigation. Xiao Liu would like to thank the China Scholarship Council (File No. 201206890019) for the financial support. Ekaterina Koposova would like to thank the St. Petersburg State University (Event 6, Project No. 12.42.1264.2014) for the financial support.

Notes and references

1 H. Ghadimi, M. R. Mahmoudian and W. J. Basirun, *RSC Adv.*, 2015, **5,** 39366-39374.
2 D. R. Rolison, *Science*, 2003, **299,** 1698-1701.
3 X. Teng, X. Liang, S. Maksimuk and H. Yang, *Small*, 2006, **2,** 249-253.
4 P. J. Cameron, L. M. Peter, S. M. Zakeeruddin and M. Grätzel, *Coord. Chem. Rev.*, 2004, **248,** 1447-1453.
5 X. Fang, T. Ma, G. Guan, M. Akiyama and E. Abe, *J. Photochem. Photobiol. A*, 2004, **164,** 179-182.
6 T. S. Ahmadi, Z. L. Wang, T. C. Green, A. Henglein and M. A. El-Sayed, *Science*, 1996, **272,** 1924-1925.
7 R. Narayanan and M. A. El-Sayed, *Nano Lett.*, 2004, **4,** 1343-1348.
8 R. Xie, Y. Pan and H. Gu, *RSC Adv.*, 2015, **5,** 16497-16500.
9 F. Li, Y. Guo, Y. Liu, J. Yan, W. Wang and J. Gao, *Carbon*, 2014, **67,** 617-626.
10 A. M. Levendorf, D.-J. Chen, C. L. Rom, Y. Liu and Y. J. Tong, *RSC Adv.*, 2014, **4,** 21284-21293.
11 H. Song, F. Kim, S. Connor, G. A. Somorjai and P. Yang, *J. Phys. Chem. B*, 2005, **109,** 188-193.
12 J. Ren and R. D. Tilley, *J. Am. Chem. Soc.*, 2007, **129,** 3287-3291.
13 Y. Song, R. M. Garcia, R. M. Dorin, H. Wang, Y. Qiu, E. N. Coker, W. A. Steen, J. E. Miller and J. A. Shelnutt, *Nano Lett.*, 2007, **7,** 3650-3655.
14 J. Chen, T. Herricks and Y. Xia, *Angew. Chem. Int. Ed.*, 2005, **44,** 2589-2592.
15 N. C. Bigall, T. Härtling, M. Klose, P. Simon, L. M. Eng and A. Eychmüller, *Nano Lett.*, 2008, **8,** 4588-4592.
16 Y. Sun, B. Mayers and Y. Xia, *Adv. Mater.*, 2003, **15,** 641-646.
17 X. Teng and H. Yang, *Nano Lett.*, 2005, **5,** 885-891.
18 M. Shirai, K. Igeta and M. Arai, *Chem. Commun.*, 2000, **7,** 623-624.
19 Y. Yamauchi, A. Takai, T. Nagaura, S. Inoue and K. Kuroda, *J. Am. Chem. Soc.*, 2008, **130,** 5426-5427.
20 Q. Shen, L. Jiang, H. Zhang, Q. Min, W. Hou and J.-J. Zhu, *J. Phys. Chem. C*, 2008, **112,** 16385-16392.
21 B. Kraeutler and A. J. Bard, *J. Am. Chem. Soc.*, 1978, **100,** 4317-4318.
22 K. Kurihara and J. H. Fendler, *J. Am. Chem. Soc.*, 1983, **105,** 6152-6153.
23 M. Harada, K. Okamoto and M. Terazima, *Langmuir*, 2006, **22,** 9142-9149.
24 A. P. Alivisatos, *Science*, 2000, **289,** 736-737.
25 J. F. Banfield, S. A. Welch, H. Zhang, T. T. Ebert and R. L. Penn, *Science*, 2000, **289,** 751-754.
26 X. Liu, D. G. Stroppa, M. Heggen, Y. Ermolenko, A. Offenhäusser and Y. Mourzina, *J. Phys. Chem. C*, 2015, **119,** 10336-10344.
27 T. A. Witten and L. M. Sander, *Phys. Rev. Lett.*, 1981, **47,** 1400-1403.
28 E. Formo, Z. Peng, E. Lee, X. Lu, H. Yang and Y. Xia, *J. Phys. Chem. C*, 2008, **112**, 9970-9975.
29 J. Wang and G. M. Swain, *J. Electrochem. Soc.*, 2003, **150**, E24-E32.
30 M. S. Faber and S. Jin, *Energy & Environmental Science*, 2014, **7,** 3519-3542.
31 J. K. Nørskov, T. Bligaard, A. Logadottir, J. R. Kitchin, J. G. Chen, S. Pandelov and U. Stimming, *J. Electrochem. Soc.*, 2005, **152**, J23-J26.
32 J. O. M. Bockris, I. A. Ammar and A. K. M. S. Huq, *J. Phys. Chem.*, 1957, **61,** 879-886.
33 J. R. McKone, E. L. Warren, M. J. Bierman, S. W. Boettcher, B. S. Brunschwig, N. S. Lewis and H. B. Gray, *Energy & Environmental Science*, 2011, **4,** 3573-3583.
34 D. V. Esposito, S. T. Hunt, A. L. Stottlemyer, K. D. Dobson, B. E. McCandless, R. W. Birkmire and J. G. Chen, *Angew. Chem. Int. Ed.*, 2010, **122,** 10055-10058.
35 R. F. Mann and C. P. Thurgood, *J. Power Sources*, 2011, **196,** 4705-4713.
36 M. G. Walter, E. L. Warren, J. R. McKone, S. W. Boettcher, Q. Mi, E. A. Santori and N. S. Lewis, *Chem. Rev.*, 2010, **110,** 6446-6473.
37 T. A. Witten and L. M. Sander, *Phys. Rev. Lett.*, 1981, **47,** 1400-1403.
38 D. Zhang, J. Li, J. Wang, S. Chen, J. Zhou, T. Li, J. Zhang, A. Zhang and C. Liu, *RSC Adv.*, 2013, **3,** 17073-17080.
39 B. Lim and Y. Xia, *Angew. Chem. Int. Ed.*, 2011, **50,** 76-85.
40 J. O'M. Bockris and A. R. Despic, *Physical Chemistry - An Advanced Treatise*, Vol. IXB, H. Eyring, D. Henderson and W. Jost (Eds.), Academic Press, New York, 1970, p. 611-724.
41 K. Manthiram, Y. Surendranath and A. P. Alivisatos, *J. Am. Chem. Soc.*, 2014, **136,** 7237-7240.
42 K. Yamada, K. Miyazaki, S. Koji, Y. Okumura and M. Shibata, *J. Power Sources*, 2008, **180**, 181-184.
43 Y. Song, Y. Yang, C. J. Medforth, E. Pereira, A. K. Singh, H. Xu, Y. Jiang, C. J. Brinker, F. van Swol and J. A. Shelnutt, *J. Am. Chem. Soc.*, 2004, **126,** 635-645.
44 J. Wang, X.-B. Zhang, Z.-L. Wang, L.-M. Wang, W. Xing and X. Liu, *Nanoscale*, 2012, **4,** 1549-1552.
45 E. Borgarello, J. Kiwi, E. Pelizzetti, M. Visca and M. Gratzel, *Nature*, 1981, **289,** 158-160.
46 M. Watabe, M. Kai, S. Asanuma, M. Yoshikane, A. Horiuchi, A. Ogasawara, T. Watanabe, T. Mikami and T. Matsumoto, *Inorg. Chem.*, 2001, **40,** 1496-1500.
47 X. Sun, S. Dong and E. Wang, *J. Am. Chem. Soc.*, 2005, **127,** 13102-13103.
48 Z. Wang, L. E. Lybarger, W. Wang, C. J. Medforth, J. E. Miller and J. A. Shelnutt, *Nanotechnology*, 2008, **19,** 395604-345609.